CHAPTER IV
RESULTS AND DISCUSSION

4.1 ITQ-21 Zeolite Synthesis and Characterizations

This section is devoted to the catalyst characterization results. The synthesized ITQ-21 zeolite was characterized using X-ray diffraction (XRD), SEM and TEM. The catalysts characteristics will be used to explain the activity of the catalysts in the next section.

4.1.1 X-ray Diffraction (XRD)

ITQ-21 zeolite was synthesized using N(16)-methyl-sparteinium cation as the organic structure-directing agent, fluoride anion as the hydrolyzing agent, and germanium oxide as the source of Al, Si and Ge, respectively. The gel mixture was stirred at room temperature until complete hydrolysis (three days) before adding a hydrofluoric acid solution and stirring for one day. The mixture was homogenized by mechanical stirring and hydrothermal conditions in a teflon-lined stainless steel autoclave at 175°C for three days. Then, the sample was washed with DI water, dried at 110°C, and finally calcined at 500°C for three hours (adapted fromArribas, M.A., Corma, A., *et al.,* 2004). The XRD pattern of the zeolite is illustrated in Figure 4.1.

It was found that the XRD pattern of the synthesized zeolite matched with that of ITQ-21 as reported by Canos et al. (2004). Therefore, it can be implied that the ITQ-21 zeolte was successfully synthesized in this study.

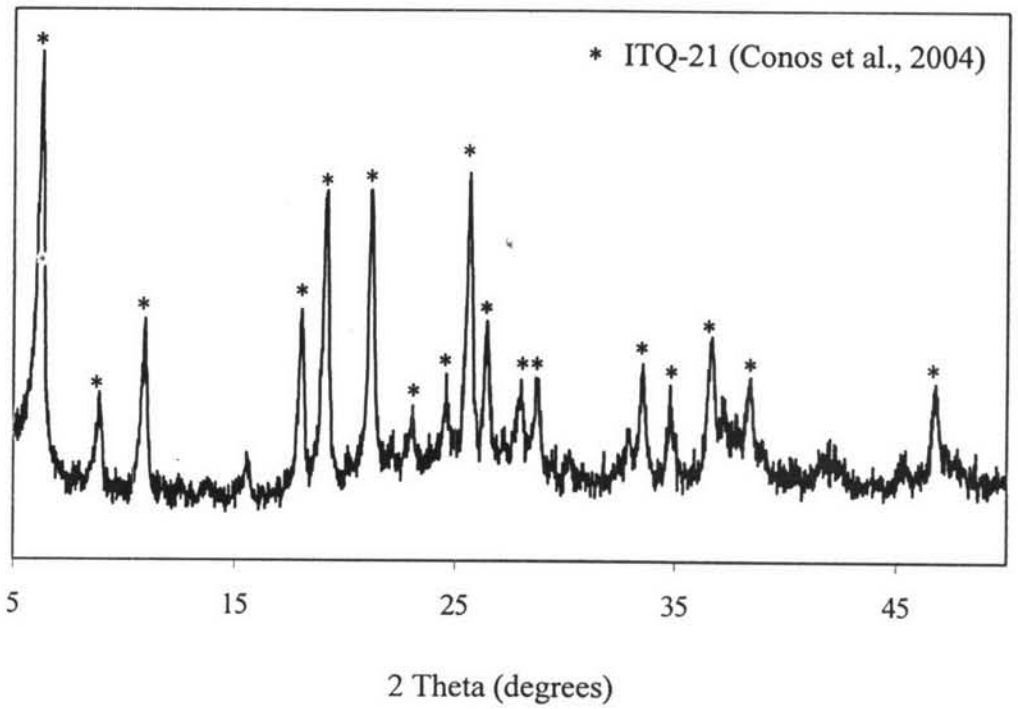

Figure 4.1 XRD pattern of synthesized ITQ-21 zeolite.

4.1.2 Scanning Electron Microscope (SEM)

Figure 4.2 shows the SEM micrograph of the synthesized ITQ-21 zeolite. It was observed that the morphology of the zeolite cannot be clearly depicted using SEM technique. The picture appears to be loose clusters of little crystallites. Also, the XRD pattern indicates the crystalline structure of the synthesized zeolite. Therefore, ITQ-21 zeolite was possibly composed of little crystallites in nano-sizes under the synthesis conditions.

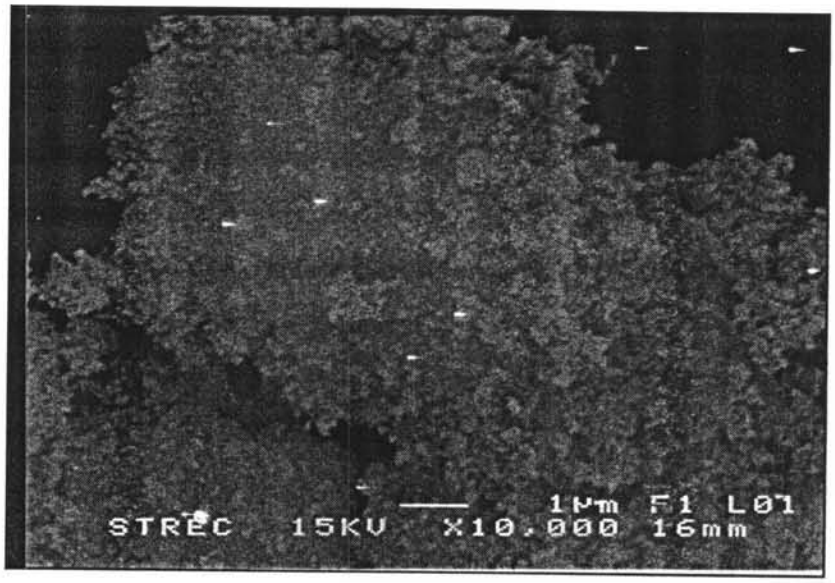

Figure 4.2 SEM micrograph of the ITQ-21 zeolite.

4.1.3 Transmission Electron Microscope (TEM)

In order to clearly observe the morphology of the synthesized zeolite, TEM technique was employed. Figure 4.3 shows the TEM image of the zeolite. The result confirms the previous conclusion that the zeolite was formed from very small crystals in nano-scales. The square shape of ITQ-21 with the average particle size of 53 nm can be obtained from the synthesis conditions.

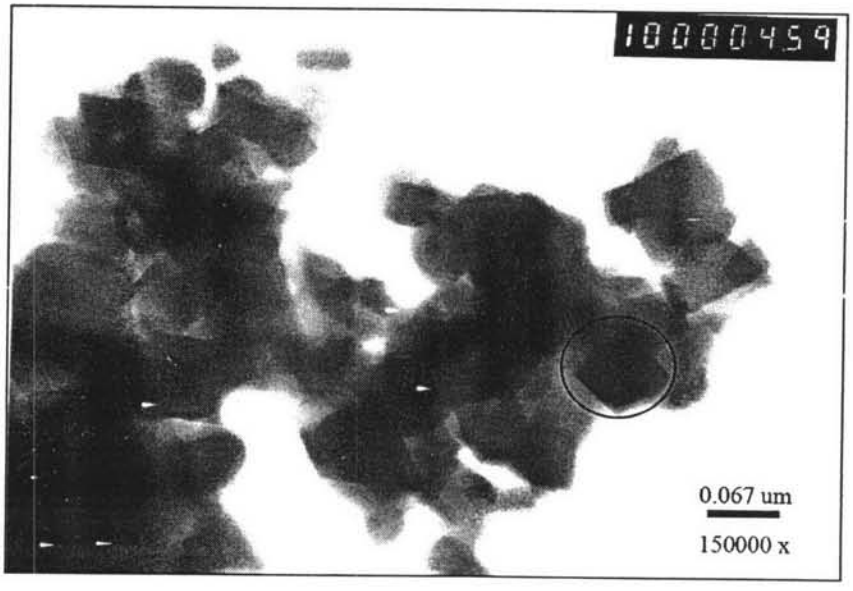

Figure 4.3 TEM micrograph of the ITQ-21 zeolite.

4.2 Activity Testing

This section presents the catalytic activity results of the prepared catalysts. Twenty-one Pd-based catalysts on the γ-Al_2O_3 support loaded with the promoters (Zr, Ti and Sn) in mono-, bi- and tri-element systems were prepared following the right-angle triangle tertiary diagram, as shown in Table 4.1 and Figure 4.1.

Table 4.1 Catalyst formulations of the palladium (Pd)-based catalysts promoted with Zr, Ti, and Sn in mono-, bi-, and tri-element systems

No.	Catalyst	% elemental loading			
		Pd	Sn	Ti	Zr
1	$C01^M$	4	-	1	-
2	$C02^B$	4	-	0.8	0.2
3	$C03^B$	4	-	0.6	0.4
4	$C04^B$	4	-	0.4	0.6
5	$C05^B$	4	-	0.2	0.8
6	$C06^M$	4	-	-	1
7	$C07^B$	4	0.2	0.8	-
8	$C08^T$	4	0.2	0.6	0.2
9	$C09^T$	4	0.2	0.4	0.4
10	$C10^T$	4	0.2	0.2	0.6
11	$C11^B$	4	0.2	-	0.8
12	$C12^B$	4	0.4	0.6	-
13	$C13^T$	4	0.4	0.4	0.2
14	$C14^T$	4	0.4	0.2	0.4
15	$C15^B$	4	0.4	-	0.6
16	$C16^B$	4	0.6	0.4	-
17	$C17^T$	4	0.6	0.2	0.2
18	$C18^B$	4	0.6	-	0.4
19	$C19^B$	4	0.8	0.2	-

20	C20[B]	4	0.8	-	0.2
21	C21[M]	4	1	-	-
22	C22[•]	4	-	-	-

Note: [M]4% Pd-based catalysts with mono-elemental promoters

[B]4% Pd-based catalysts with bi-elemental promoters (Pd/Sn/Ti, Pd/Sn/Zr, Pd/Ti/Zr)

[T]4% Pd-based catalysts with tri-elemental promoters (Pd/Sn/Ti/Zr)

[•]unpromoted 4% Pd catalyst

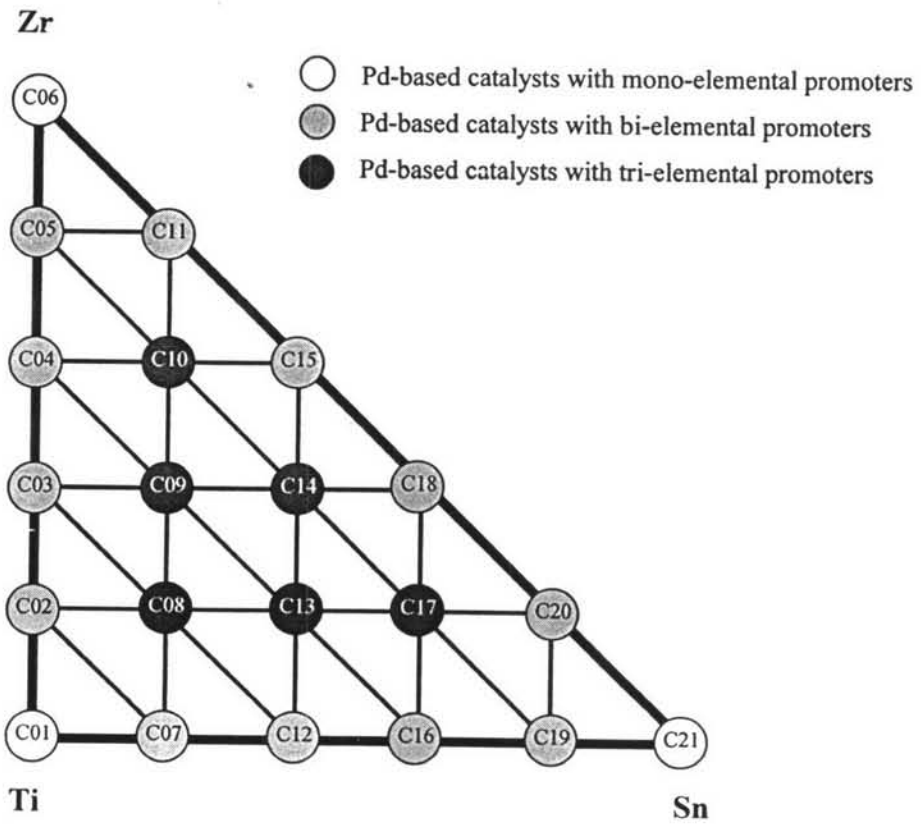

Figure 4.4 Right-angled triangle tertiary diagram to represent a schematic of the catalysts.

4.2.1 Effect of Promoters

For investigating the combustion activity of the employed catalysts, the experiments were performed under the temperatures of 450, 500, 550, 600, and 650°C.

Conversions along the time-on-stream at different temperatures for all the catalyst members are shown in Figures 4.5 to 4.26 by the identified order.

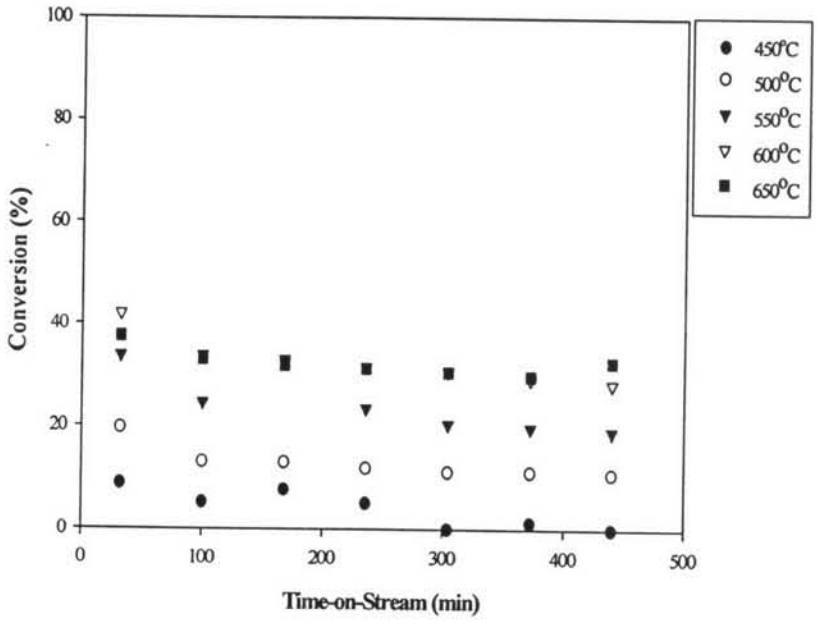

Figure 4.5 Methane conversion of the γ-alumina-supported catalyst promoted with 4%Pd and 1%Ti (C01) at different temperatures.

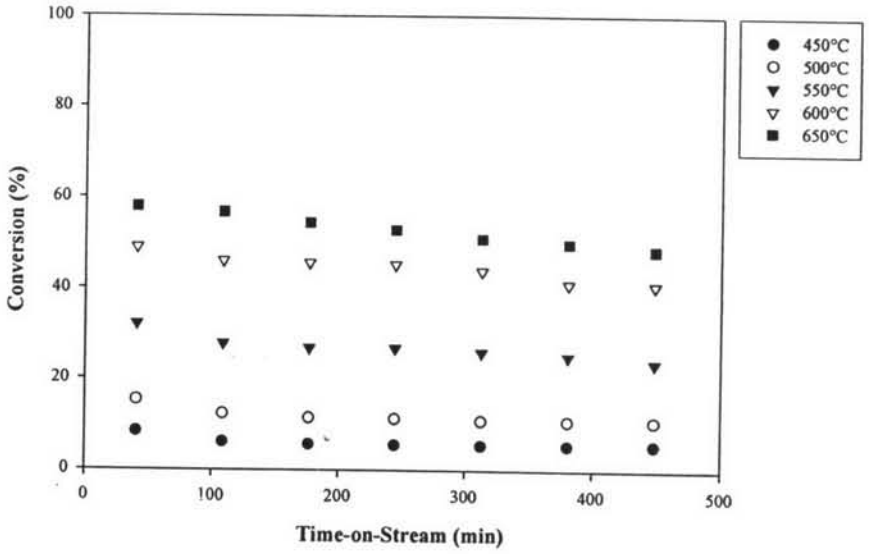

Figure 4.6 Methane conversion of the γ-alumina-supported catalyst promoted with 4%Pd, 0.8%Ti, and 0.2%Zr (C02) at different temperatures.

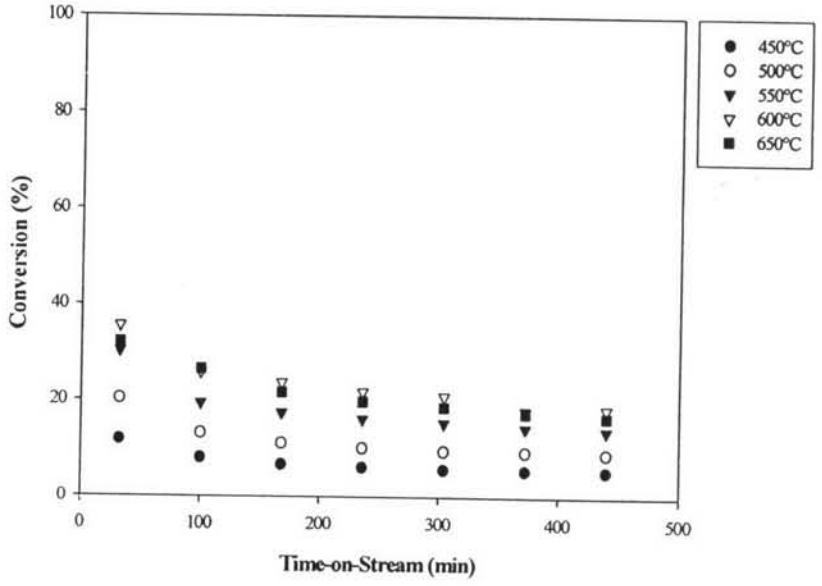

Figure 4.7 Methane conversion of the γ-alumina-supported catalyst promoted with 4%Pd, 0.6%Ti, and 0.4%Zr (C03) at different temperatures.

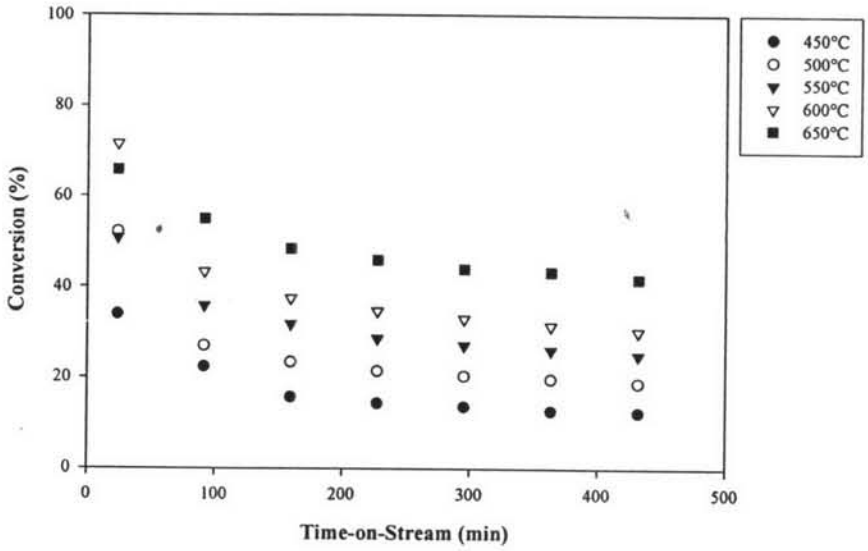

Figure 4.8 Methane conversion of the γ-alumina-supported catalyst promoted with 4%Pd, 0.4%Ti, and 0.6%Zr (C04) at different temperatures.

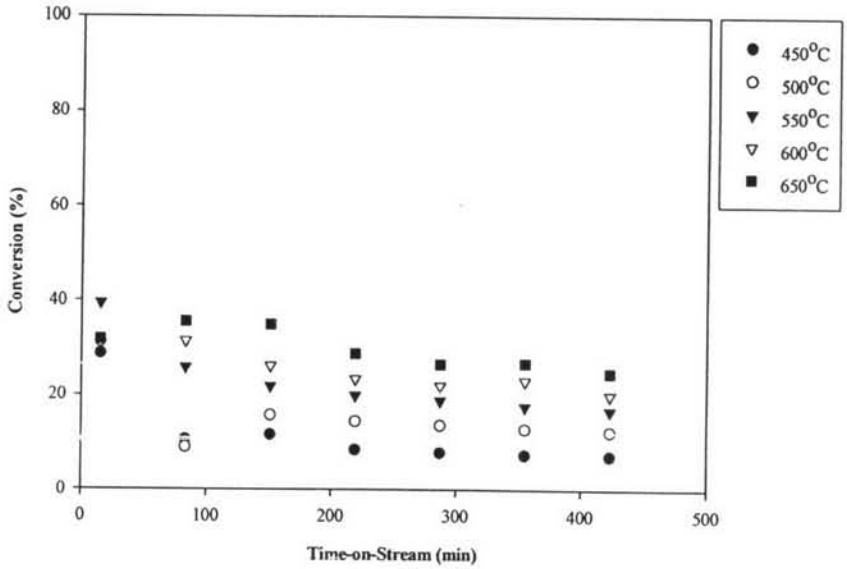

Figure 4.9 Methane conversion of the γ-alumina-supported catalyst promoted with 4%Pd, 0.2%Ti, and 0.8%Zr (C05) at different temperatures.

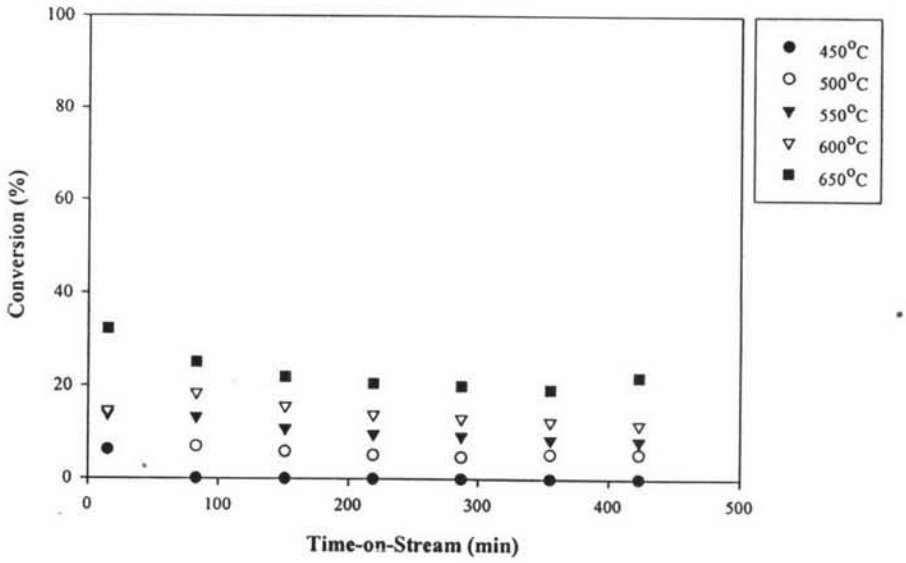

Figure 4.10 Methane conversion of the γ-alumina-supported catalyst promoted with 4%Pd, and 1%Zr (C06) at different temperatures.

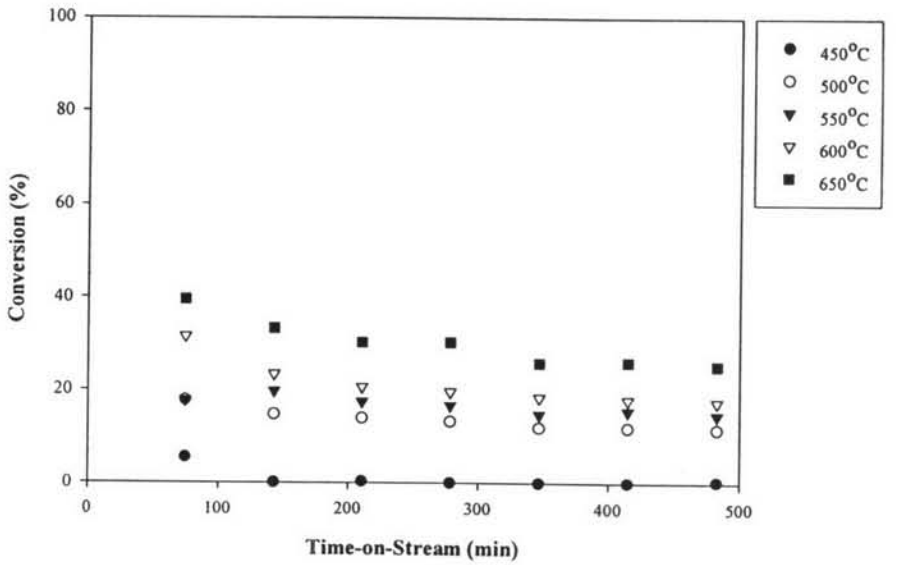

Figure 4.11 Methane conversion of the γ-alumina-supported catalyst promoted with 4%Pd, 0.2%Sn, and 0.8%Ti (C07) at different temperatures.

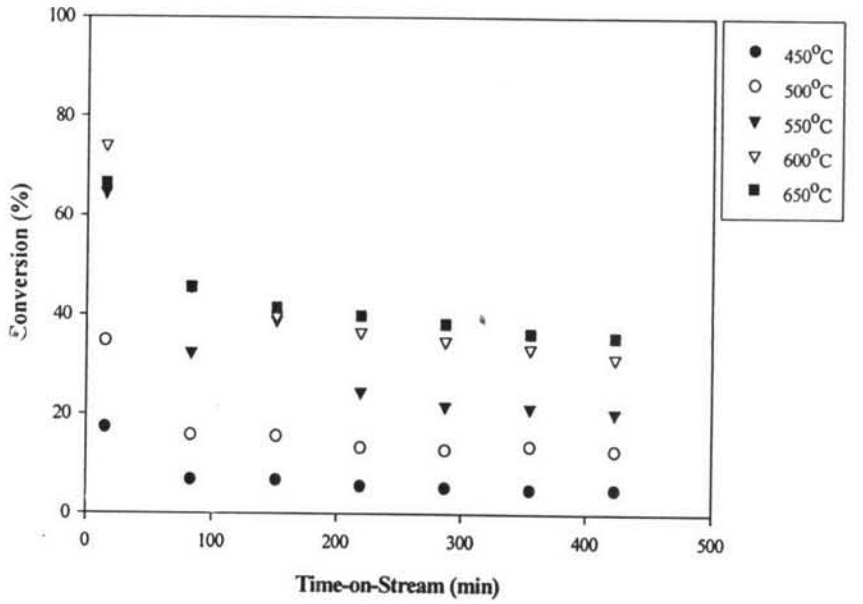

Figure 4.12 Methane conversion of the γ-alumina-supported catalyst promoted with 4%Pd, 0.2%Sn, 0.6%Ti, and 0.2%Zr (C08) at different temperatures.

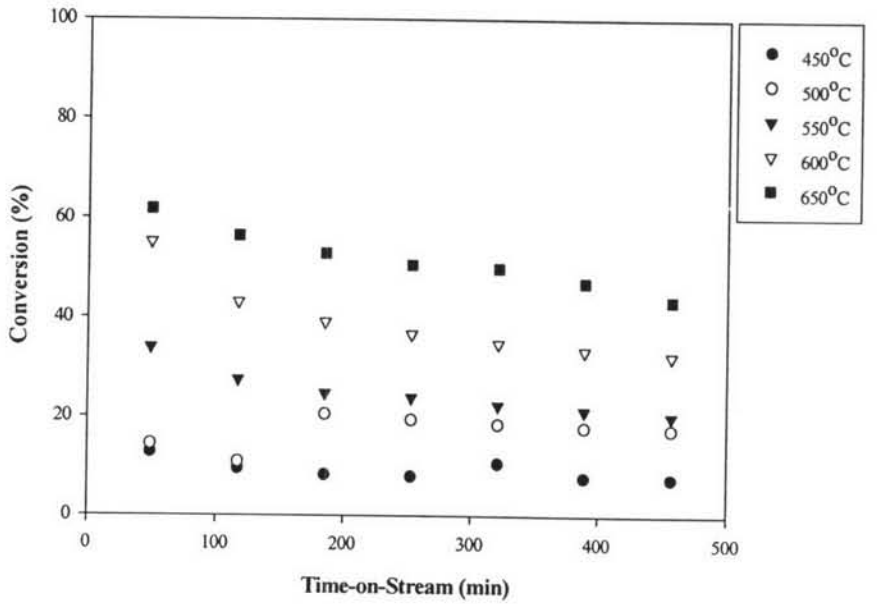

Figure 4.13 Methane conversion of the γ-alumina-supported catalyst promoted with 4%Pd, 0.2%Sn, 0.4%Ti, and 0.4%Zr (C09) at different temperatures.

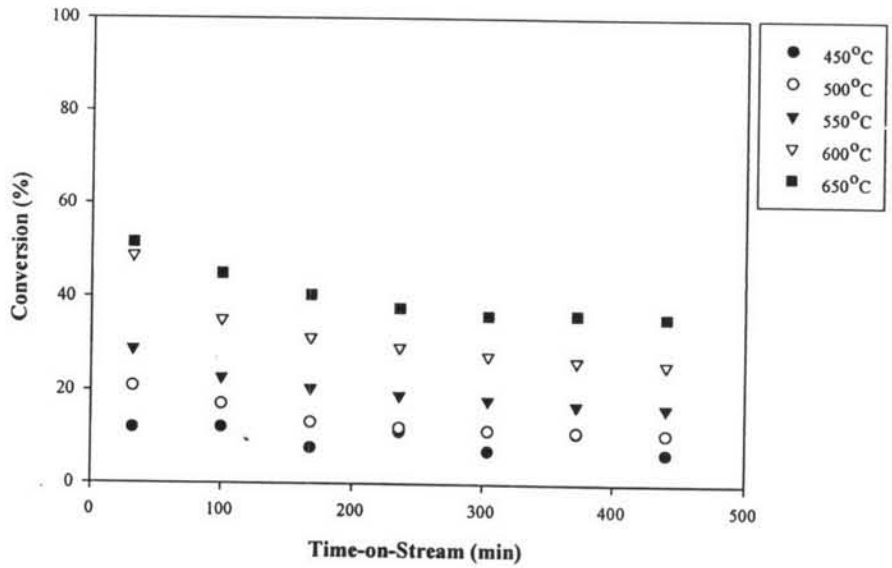

Figure 4.14 Methane conversion of the γ-alumina-supported catalyst promoted with 4%Pd, 0.2%Sn, 0.2%Ti, and 0.6%Zr (C10) at different temperatures.

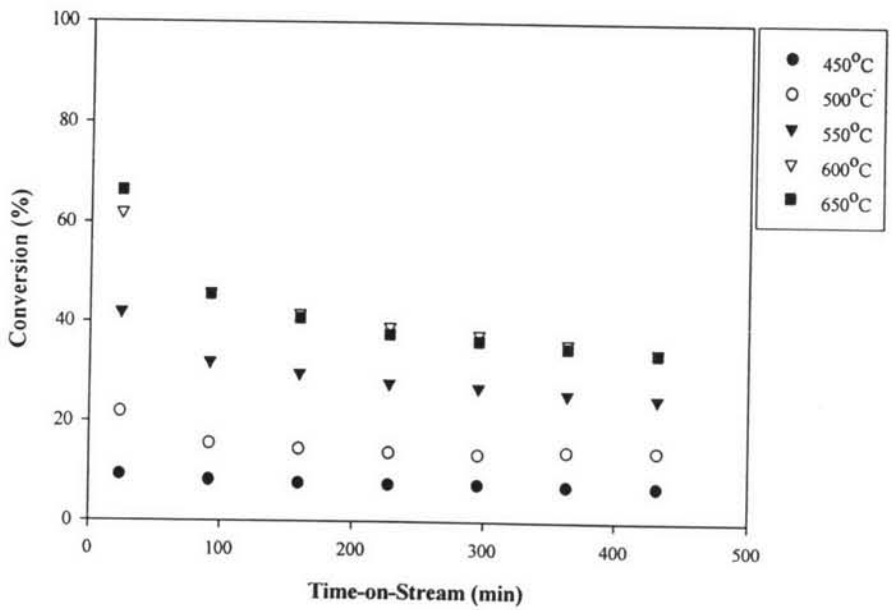

Figure 4.15 Methane conversion of the γ-alumina-supported catalyst promoted with 4%Pd, 0.2%Sn, and 0.8%Zr (C11) at different temperatures.

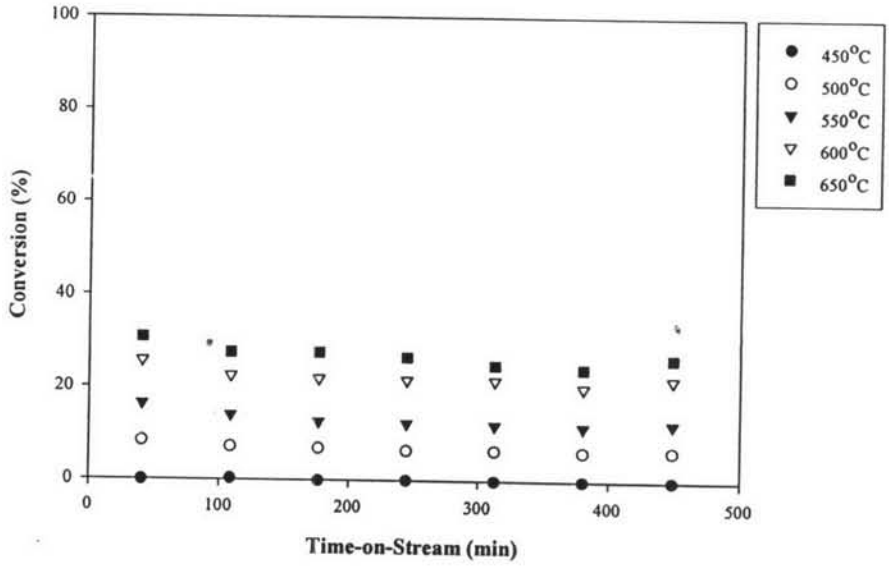

Figure 4.16 Methane conversion of the γ-alumina-supported catalyst promoted with 4%Pd, 0.4%Sn, and 0.6%Ti (C12) at different temperatures.

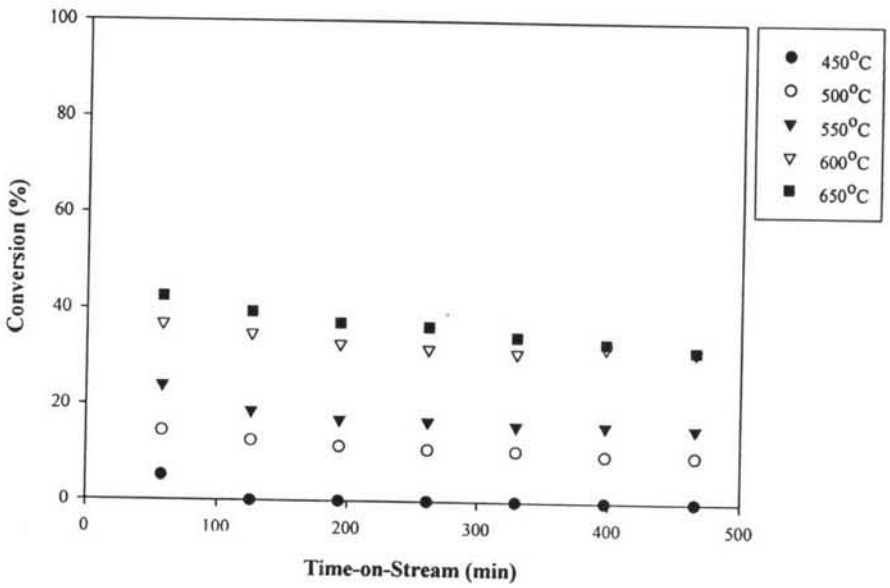

Figure 4.17 Methane conversion of the γ-alumina-supported catalyst promoted with 4%Pd, 0.4%Sn, 0.4%Ti, and 0.2%Zr (C13) at different temperatures.

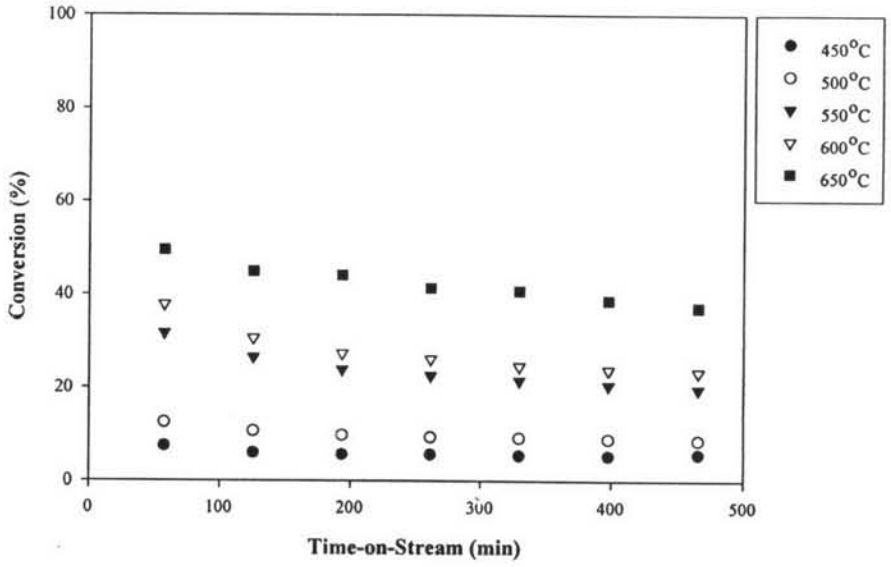

Figure 4.18 Methane conversion of the γ-alumina-supported catalyst promoted with 4%Pd, 0.4%Sn, 0.2%Ti, and 0.4%Zr (C14) at different temperatures.

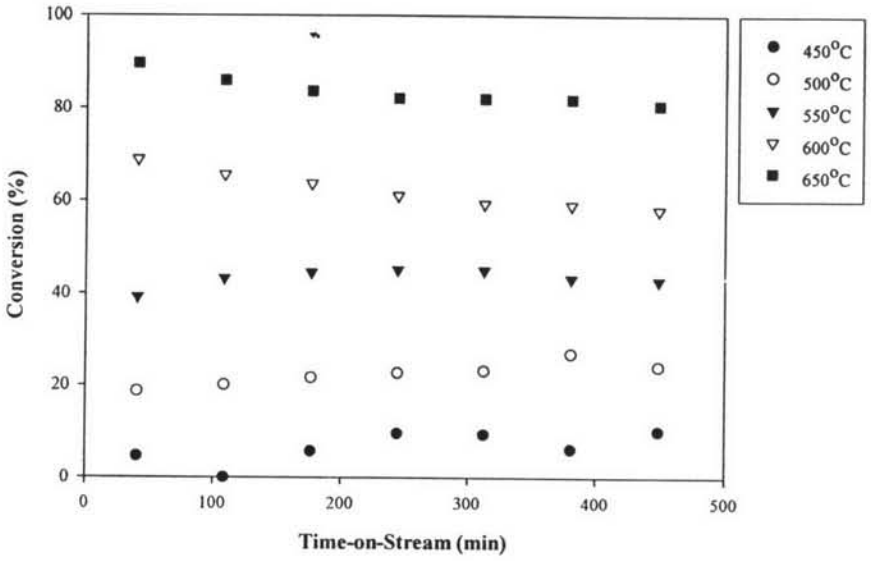

Figure 4.19 Methane conversion of the γ-alumina-supported catalyst promoted with 4%Pd, 0.4%Sn, and 0.6%Zr (C15) at different temperatures.

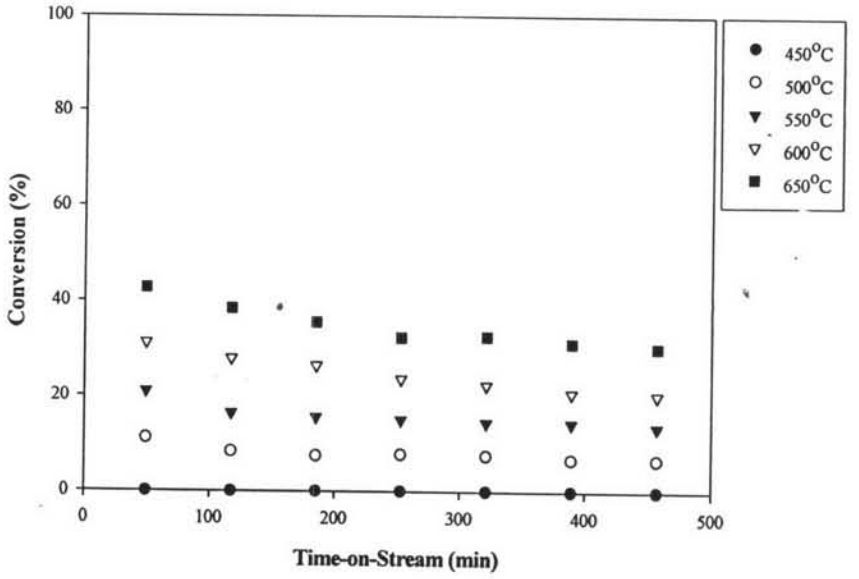

Figure 4.20 Methane conversion of the γ-alumina-supported catalyst promoted with 4%Pd, 0.4%Sn, and 0.4%Ti (C16) at different temperatures.

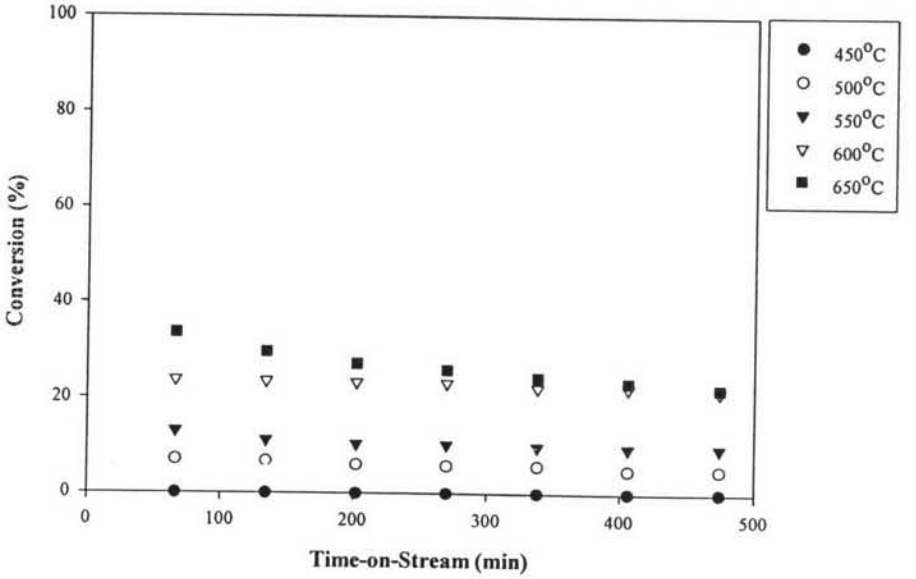

Figure 4.21 Methane conversion of the γ-alumina-supported catalyst promoted with 4%Pd, 0.6%Sn, 0.2%Ti, and 0.2%Zr (C17) at different temperatures.

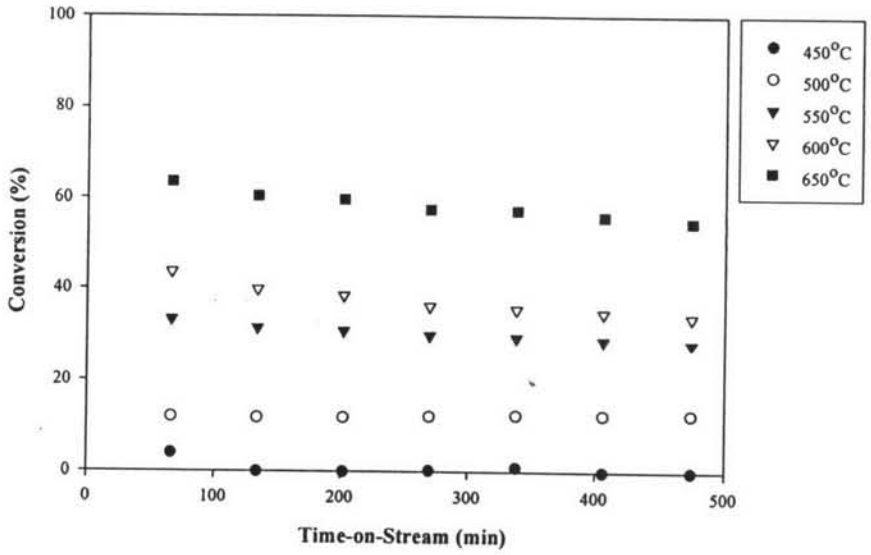

Figure 4.22 Methane conversion of the γ-alumina-supported catalyst promoted with 4%Pd, 0.6%Sn, and 0.4%Zr (C18) at different temperatures.

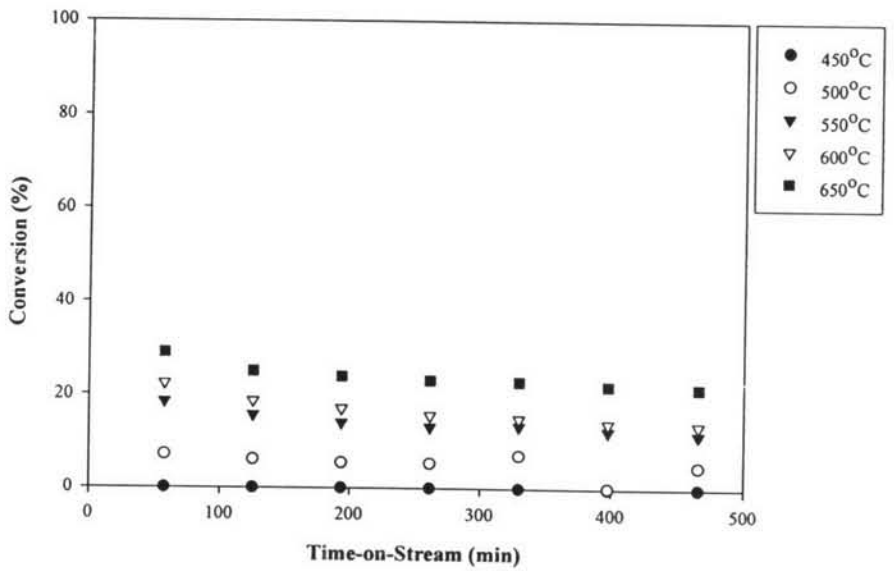

Figure 4.23 Methane conversion of the γ-alumina-supported catalyst promoted with 4%Pd, 0.8%Sn, and 0.2%Ti (C19) at different temperatures.

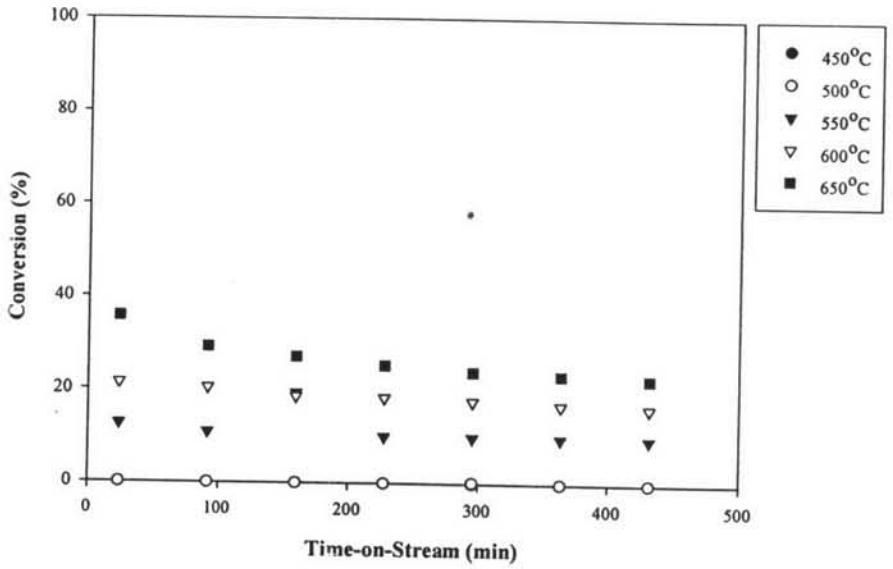

Figure 4.24 Methane conversion of the γ-alumina-supported catalyst promoted with 4%Pd, 0.8%Sn, and 0.2%Zr (C20) at different temperatures.

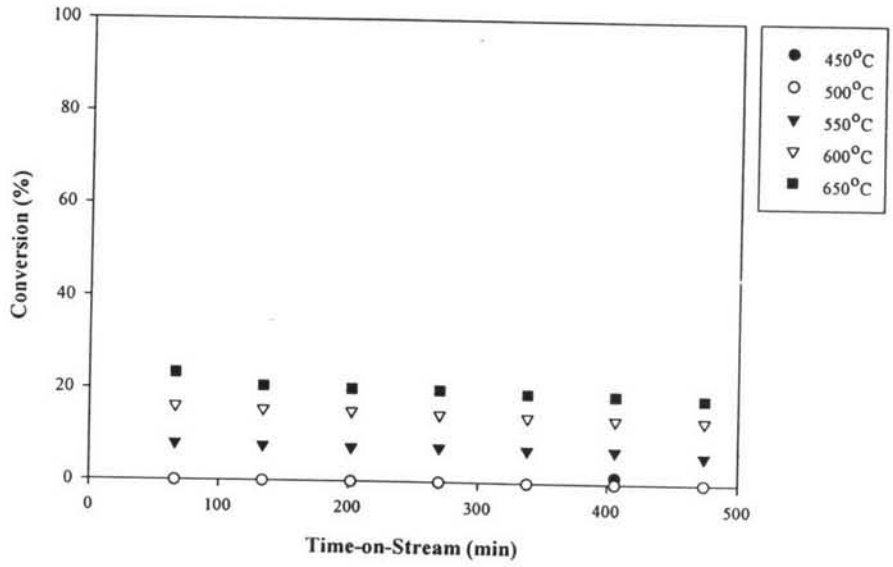

Figure 4.25 Methane conversion of the γ-alumina-supported catalyst promoted with 4%Pd, and 1%Sn (C21) at different temperatures.

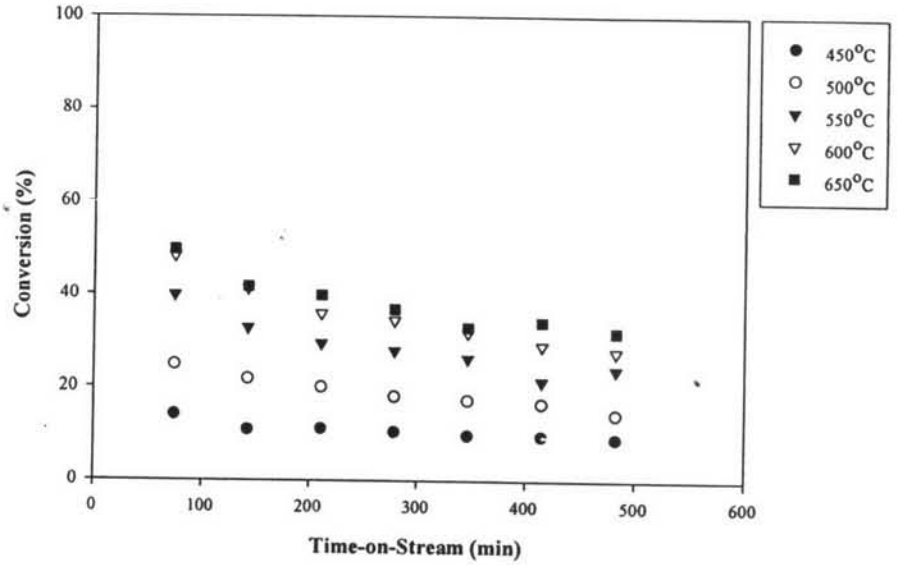

Figure 4.26 Methane conversion of the γ-alumina-supported catalyst promoted with 4%Pd (C22) at different temperatures.

The results show that the 4%Pd, 0.4%Sn, and 0.6%Zr catalyst provides the highest conversion, which also increases with increasing temperature. However, the conversion decreases with the increasing of time-on-stream.

The contour plots of steady state conversions on the right-angle triangle tertiary diagram of all catalysts were constructed at the different temperatures. Figures 4.24 to 4.28 show the contour plots of catalytic activity at various temperatures of the employed catalysts. The colors in these diagrams indicate the different conversion and active zones.

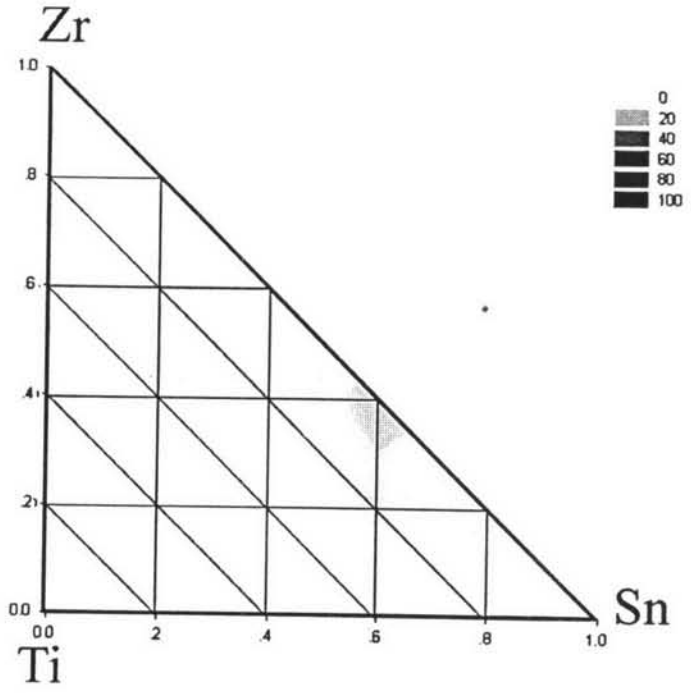

Figure 4.27 Contour plot of catalytic activity at 450°C.

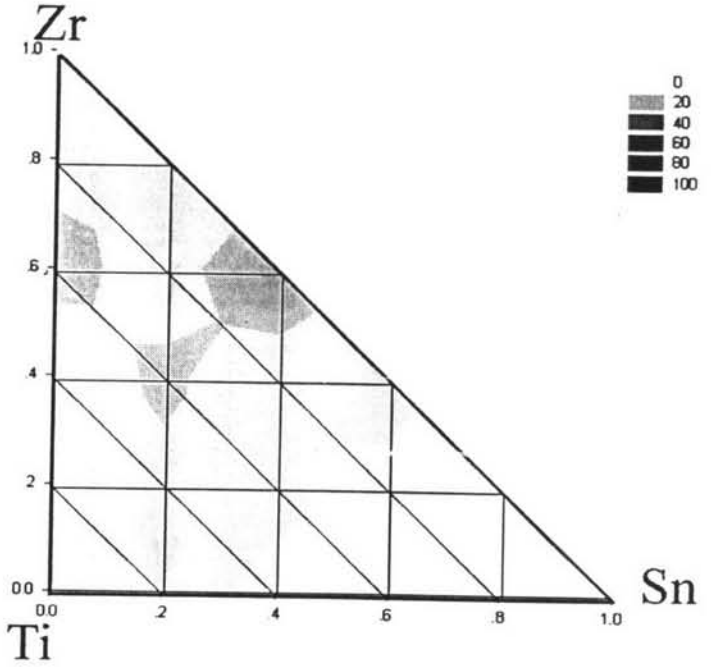

Figure 4.28 Contour plot of catalytic activity at 500°C.

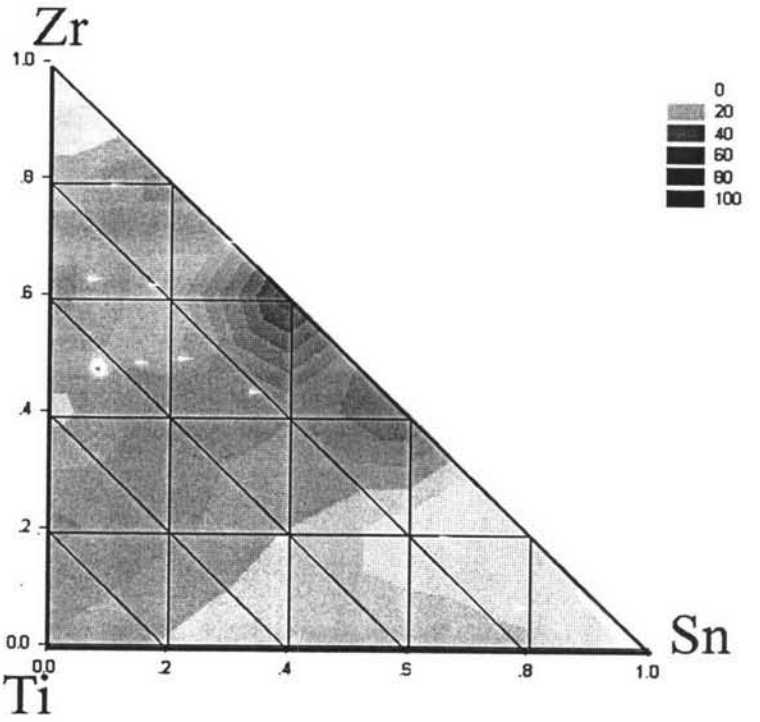

Figure 4.29 Contour plot of catalytic activity at 550°C.

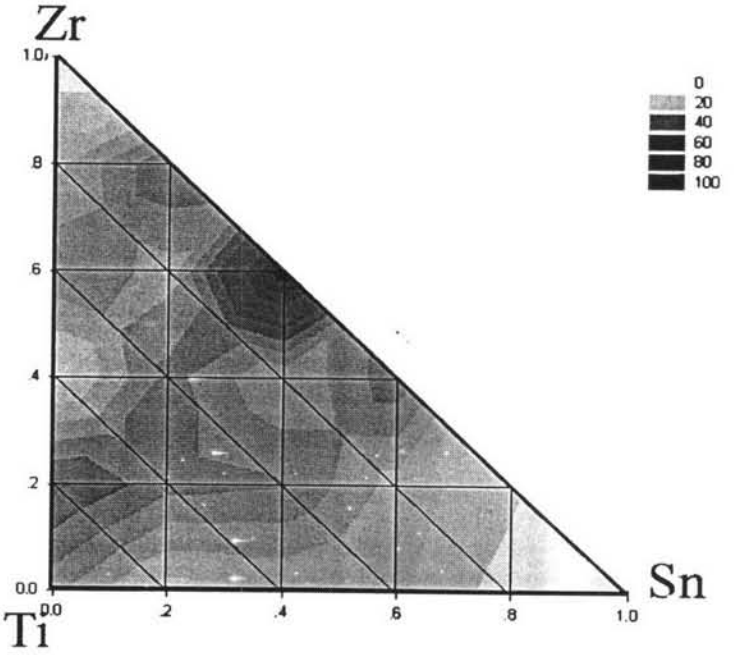

Figure 4.30 Contour plot of catalytic activity at 600°C.

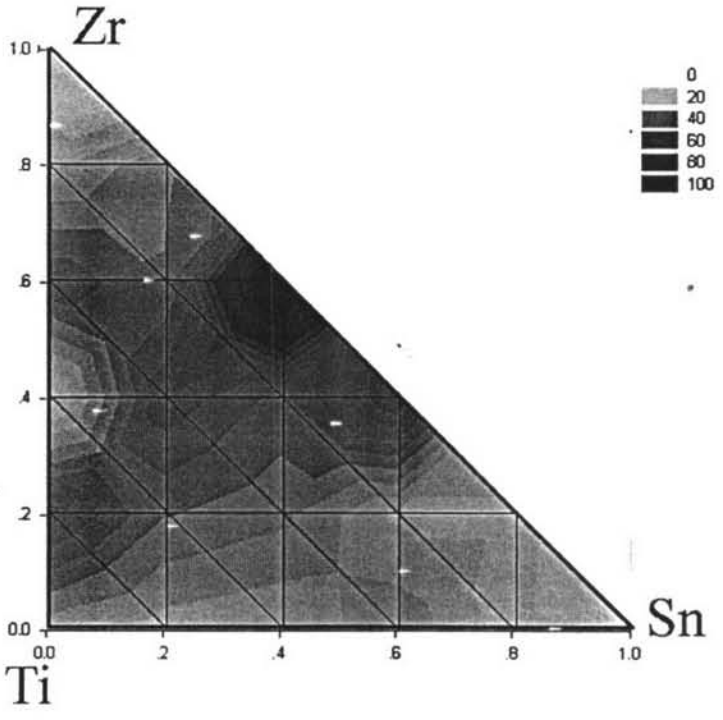

Figure 4.31 Contour plot of catalytic activity at 650°C.

It was found that, the Pd-based catalysts that were promoted in mono-element system of Zr, Ti, and Sn show the lower conversions compared with those of bi-, and tri-element promoted Pd-based catalysts. For the case of bi-element promoter, The Zr-Ti promoted catalysts showed the increase of methane conversion (C02, C03, and C04), which is in the same tendency as Zr-Sn bi-elemental promoted catalysts (C15 and C18). However, the bi-elemental Ti-Sn promoters seem to suppress the activity of the catalysts. For other case of tri-elemental promoted catalysts, a high conversion were also observed.

Table 4.2 lists the composition of the selected lead formulations. It was observed that the composition of leads contained at least Zr co-promoted with Ti or/and Sn, besides Pd that is the active metal. With comparative consideration, the effects of Zr in bi-elemental promoting system with Ti (C02, C03, and C04) and Sn (C15 and C18), and those of tri-element promoters (C09, C10, and C14) (Table 4.3) suggest that the presence of Zr in a higher amount with at least one other promoters

could slightly enhance the combustion activity of the catalysts. However, the promoter seems not to be effective when using as a promoter individually.

Table 4.2 Lead formulations selected from the activity screening results using the eight-tubular-flow reactors

No.	Catalyst	% elemental loading			
		Pd	Sn	Ti	Zr
1	C02	4	-	0.8	0.2
2	C03	4	-	0.6	0.4
3	C04	4	-	0.4	0.6
4	C09	4	0.2	0.4	0.4
5	C10	4	0.2	0.2	0.6
6	C14	4	0.4	0.2	0.4
7	C15	4	0.4	-	0.6
8	C18	4	0.6	-	0.4

For the catalysts, which were promoted with a fixed 0.4% Zr (C03, C09, C14, and C18) and 0.6%Zr (C04, C10, and C15), the substitution of Ti by Sn tended to slightly improve the combustion activity of the leads. Therefore, it can be concluded that the presence of Zr with at least one other promoter (Sn or Ti) could provide a catalyst with relative high combustion activity, particularly for Sn-Zr promoted Pd/γ-Al_2O_3 catalysts. Only the catalysts containing relatively 4%Pd, 0.4%Sn, and 0.6%Zr (C15) showed the outstanding activity around of 85% conversion at 650°C, and it was selected as the first lead.

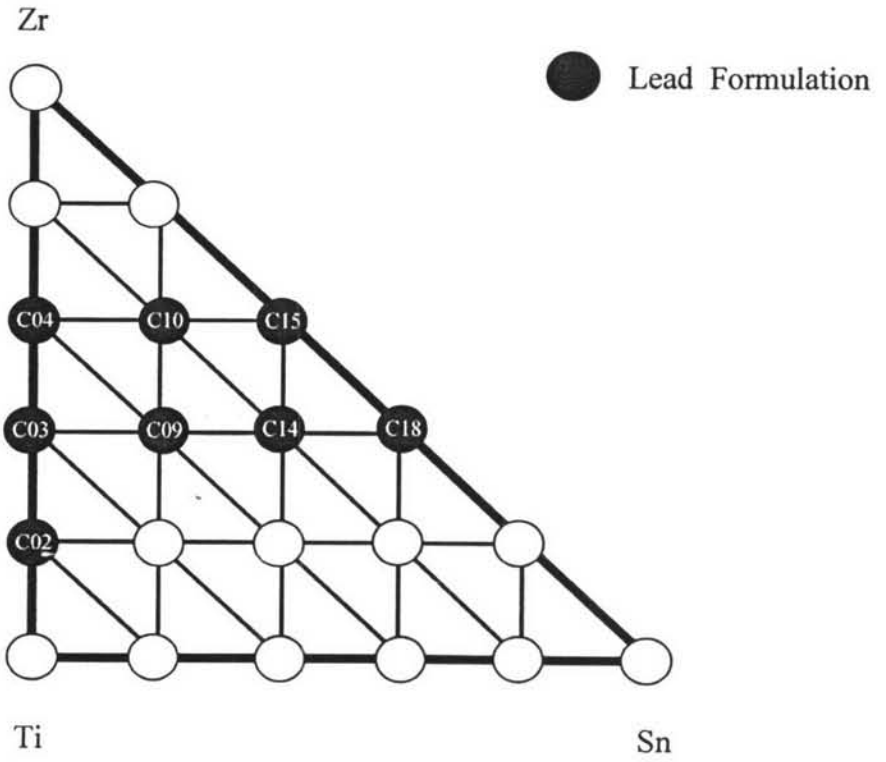

Figure 4.32 Right-angle triangle tertiary diagram representing a systematic arrangement of lead formulation.

Table 4.3 Methane conversion (%) of lead formulations supported on γ-Al_2O_3 at different temperatures

No.	Catalyst	Relative ratio of elemental Loading (%)				% Conversion at different temperature (°C)				
		Pd	Sn	Ti	Zr	450	500	550	600	650
1	C02	4	-	0.8	0.2	5.53	11.2	26.7	45.3	52.9
2	C03	4	-	0.6	0.4	60.7	10.1	16.1	21.7	19.7
3	C04	4	-	0.4	0.6	14.3	21.4	28.5	34.6	45.9
4	C09	4	0.2	0.4	0.4	8.01	19.4	23.8	36.6	50.5
5	C10	4	0.2	0.2	0.6	11.2	12.0	19.0	29.2	37.7
6	C14	4	0.4	0.2	0.4	5.60	9.29	22.4	26.1	41.3
7	C15	4	0.4	-	0.6	9.58	22.7	45.0	61.1	82.2
8	C18	4	0.6	-	0.4	0.230	12.1	29.8	36.2	57.5

4.2.2 Effect of the Catalyst Support: γ-Al_2O_3 + 5%ITQ-21

For studying the effect of ITQ-21 mixing into γ-Al_2O_3 on the combustion activity of the Sn, Ti, and Zr promoted Pd-based catalysts, the selected leads were loaded on γ-Al_2O_3 mixed with 5% ITQ-21 before being investigated for their combustion activity at 450, 500, 550, 600, and 650°C.

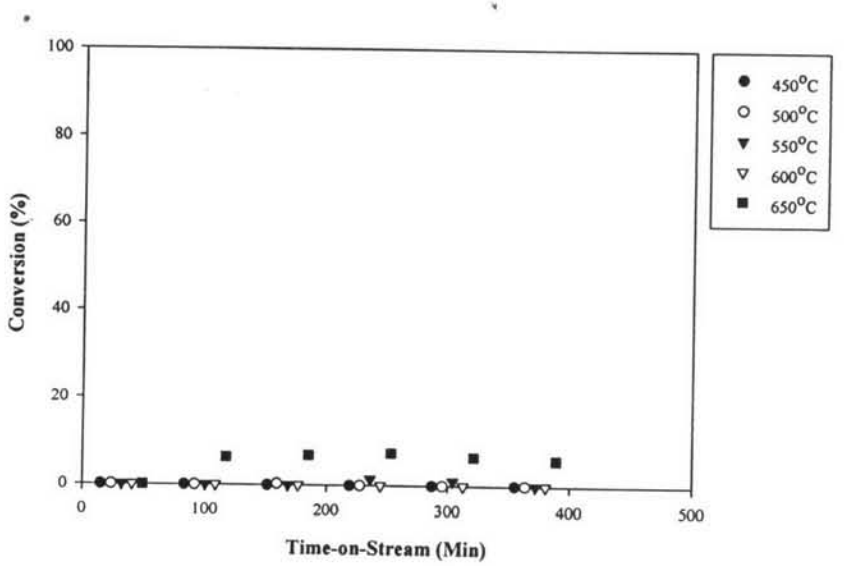

Figure 4.33 Methane conversion of the catalyst promoted with 4%Pd, 0.8%Ti, and 0.2%Zr catalysts (C02) supported on γ-Al_2O_3 mixed with 5% ITQ-21 at different temperatures.

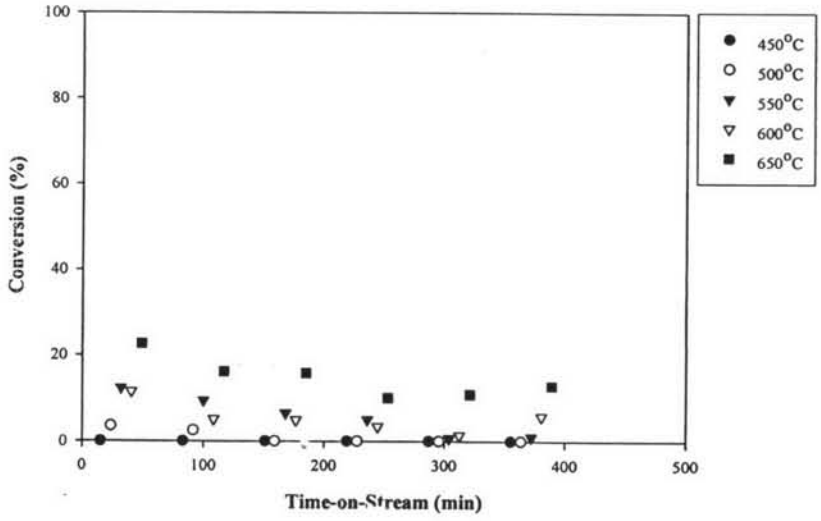

Figure 4.34 Methane conversion of the catalyst promoted with 4%Pd, 0.6%Ti, and 0.4%Zr catalysts (C03) supported on γ-Al_2O_3 mixed with 5% ITQ-21 at different temperatures.

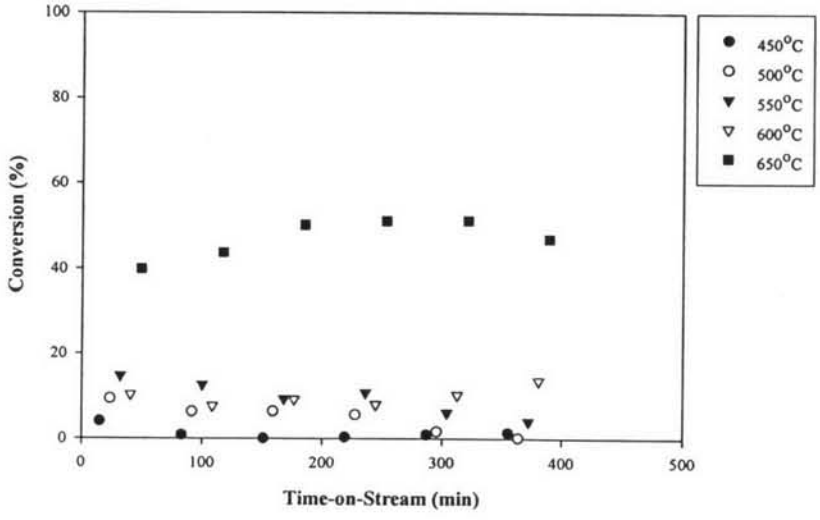

Figure 4.35 Methane conversion of the catalyst promoted with 4%Pd, 0.4%Ti, and 0.6%Zr catalysts (C04) supported on γ-Al_2O_3 mixed with 5% ITQ-21 at different temperatures.

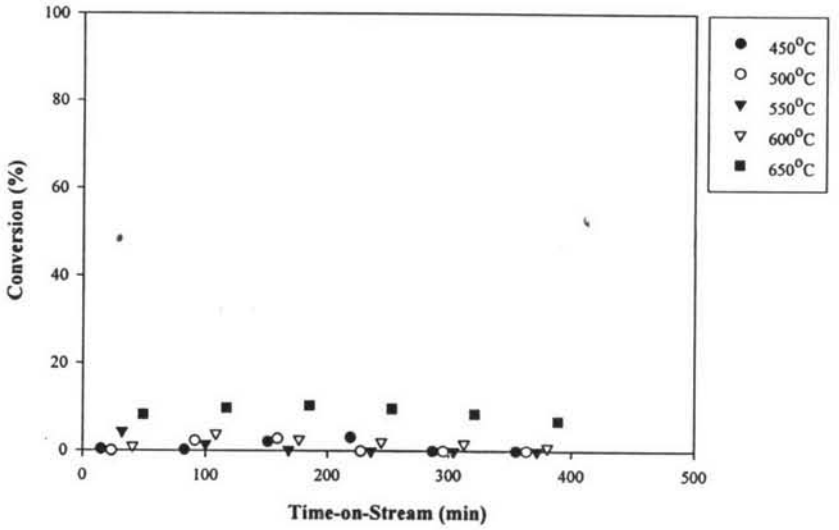

Figure 4.36 Methane conversion of the catalyst promoted with 4%Pd, 0.2%Sn, 0.4%Ti, and 0.4%Zr catalysts (C09) supported on γ-Al_2O_3 mixed with 5% ITQ-21 at different temperatures.

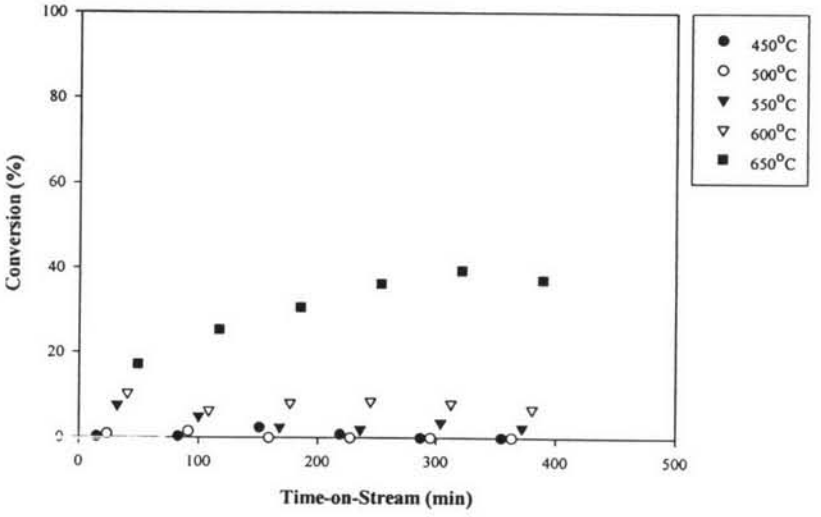

Figure 4.37 Methane conversion of the catalyst promoted with 4%Pd, 0.2%Sn, 0.2%Ti, and 0.6%Zr catalysts (C10) supported on γ-Al_2O_3 mixed with 5% ITQ-21 at different temperatures.

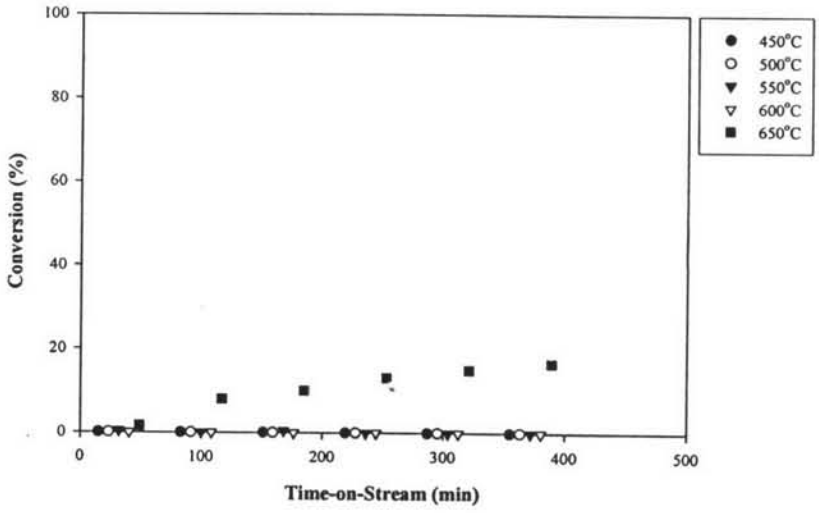

Figure 4.38 Methane conversion of the catalyst promoted with 4%Pd, 0.4%Sn, 0.2%Ti, and 0.4%Zr catalysts (C14) supported on γ-Al_2O_3 mixed with 5% ITQ-21 at different temperatures.

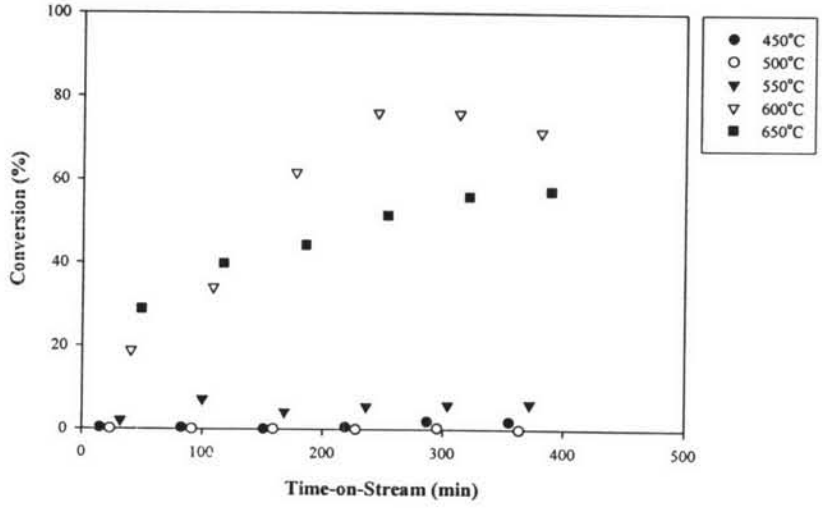

Figure 4.39 Methane conversion of the catalyst promoted with 4%Pd, 0.4%Sn, and 0.6%Zr catalysts (C15) supported on γ-Al_2O_3 mixed with 5% ITQ-21 at different temperatures.

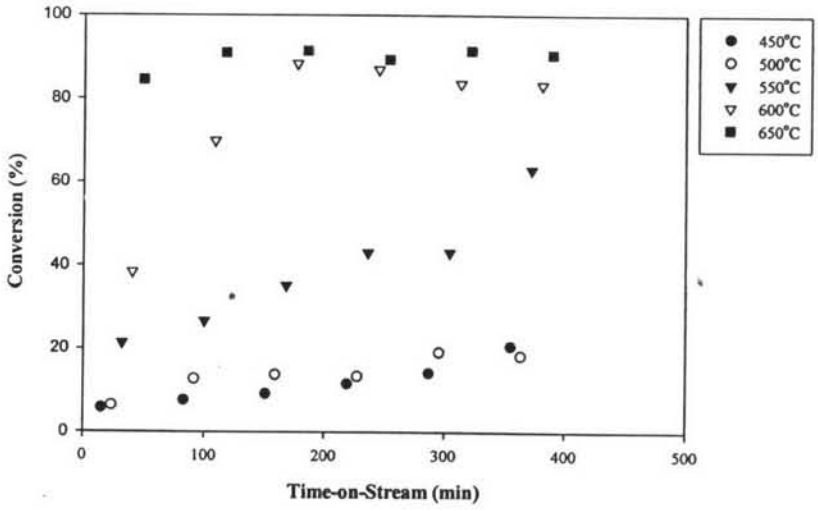

Figure 4.40 Methane conversion of the catalyst promoted with 4%Pd, 0.6%Sn, and 0.4%Zr catalysts (C18) supported on γ-Al_2O_3 mixed with 5% ITQ-21 at different temperatures.

Figures 4.33 to 4.40 illustrates the conversions of lead formulations supported on γ-Al_2O_3 mixed with ITQ-21 as a function of time-on-stream performed between 450-650°C. The results show that the combustion activity of the eight catalysts tends to be suppressed by the presence of ITQ-21.

Figure 4.41 exhibits methane conversion of the lead formulations supported on γ-Al_2O_3 and γ-Al_2O_3 mixed with ITQ-21. It was found that the addition of ITQ-21 tended to improve the catalyst stability along the testing time. Therefore, it can be concluded that the addition ITQ-21 could improve catalyst stability outweighted with the reduction of catalyst activity. Table 4.4 illustrates the conversions on different catalyst supports at 650°C. It was observed that by using ITQ-21 and γ-Al_2O_3 support mixture, the catalyst promoted with 0.6%Sn and 0.4%Zr provided higher activity than that of supported γ-Al_2O_3 catalyst.

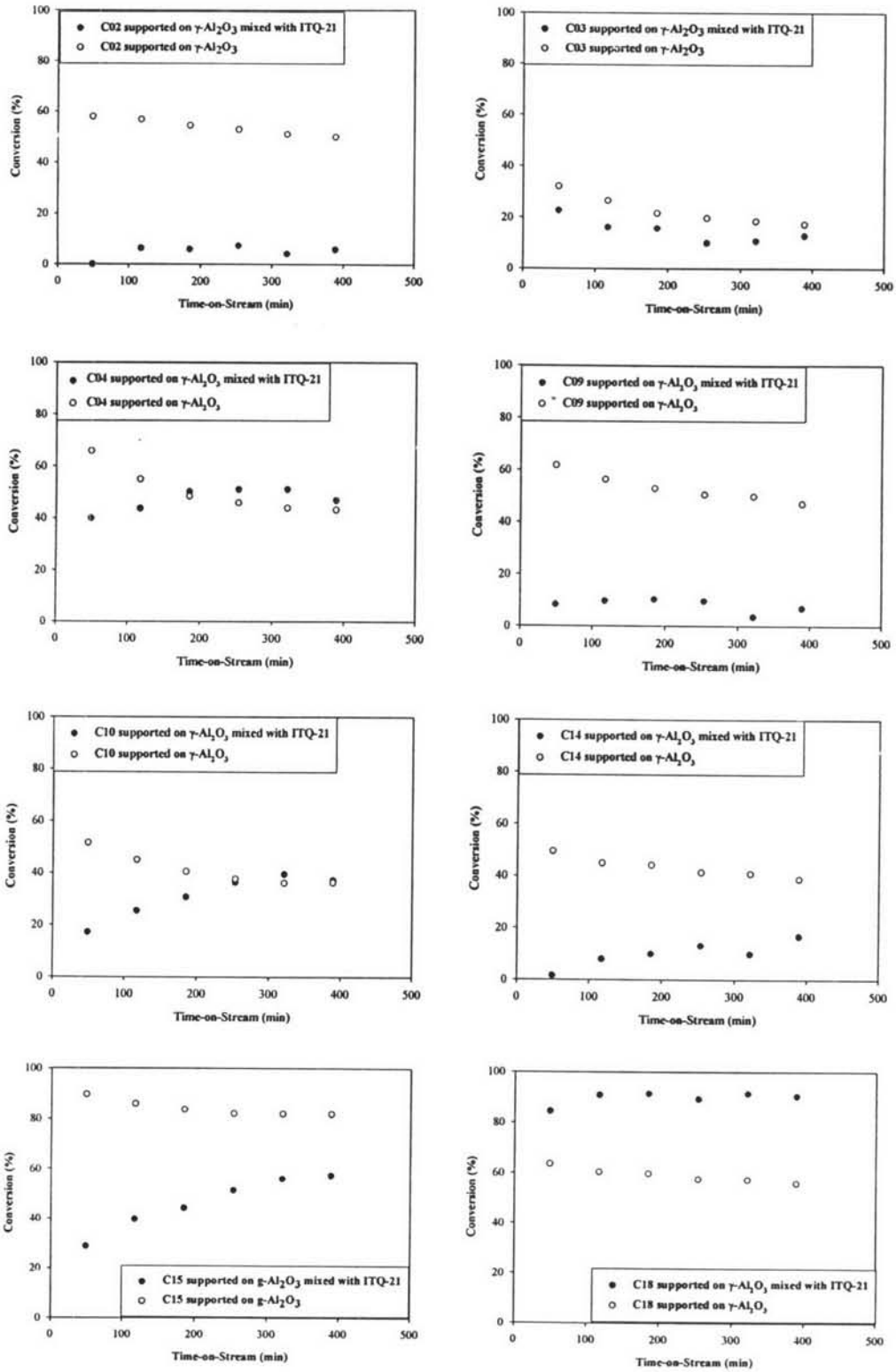

Figure 4.41 Methane conversion of the leads on two different supports at 650°C.

Table 4.4 Methane conversion (%) of the leads on to different supports at 650°C

Lead formulation	%conversion of different support at 650°C	
	γ-Al_2O_3	γ-Al_2O_3+ITQ-21
C02	52.9	5.90
C03	19.7	12.90
C04	45.9	47.0
C09	50.5	6.90
C10	37.7	37.3
C14	41.3	16.7
C15	82.1	57.4
C18	57.5	90.5

Figure 4.42 illustrates the methane conversion as a function of temperature on the different running cycles. In this study, the leads supported on the mixture of γ-Al_2O_3 and ITQ-21 catalysts were tested for their combustion activity from 450-600°C in the first cycle before being re-investigated for their combustion activity at the same temperatures in the second cycle. It was observed that the employed catalysts exhibited two different results, which can be classified into 2 groups.

The first group is the catalysts that provided the activity of the first running cycle higher than that of the second cycle (C15 and C18). It is believed that the cluster of PdO should be formed on the support during the first run. So, the activity is higher in the first cycle. During the first heating cycle, it seems that PdO would undergo agglomeration to be a bigger cluster resulting in the dramatical loss of active sites and catalyst activity.

And, the second group is the catalysts that provided the same activity for both first and second running cycle (C02, C03, C04, C09, C10, and C14). It is observed that the activity of the second testing is similar to that of the first, implying that the PdO clusters did not agglomerate on the surface because the catalysts have low activity at the first cycle.

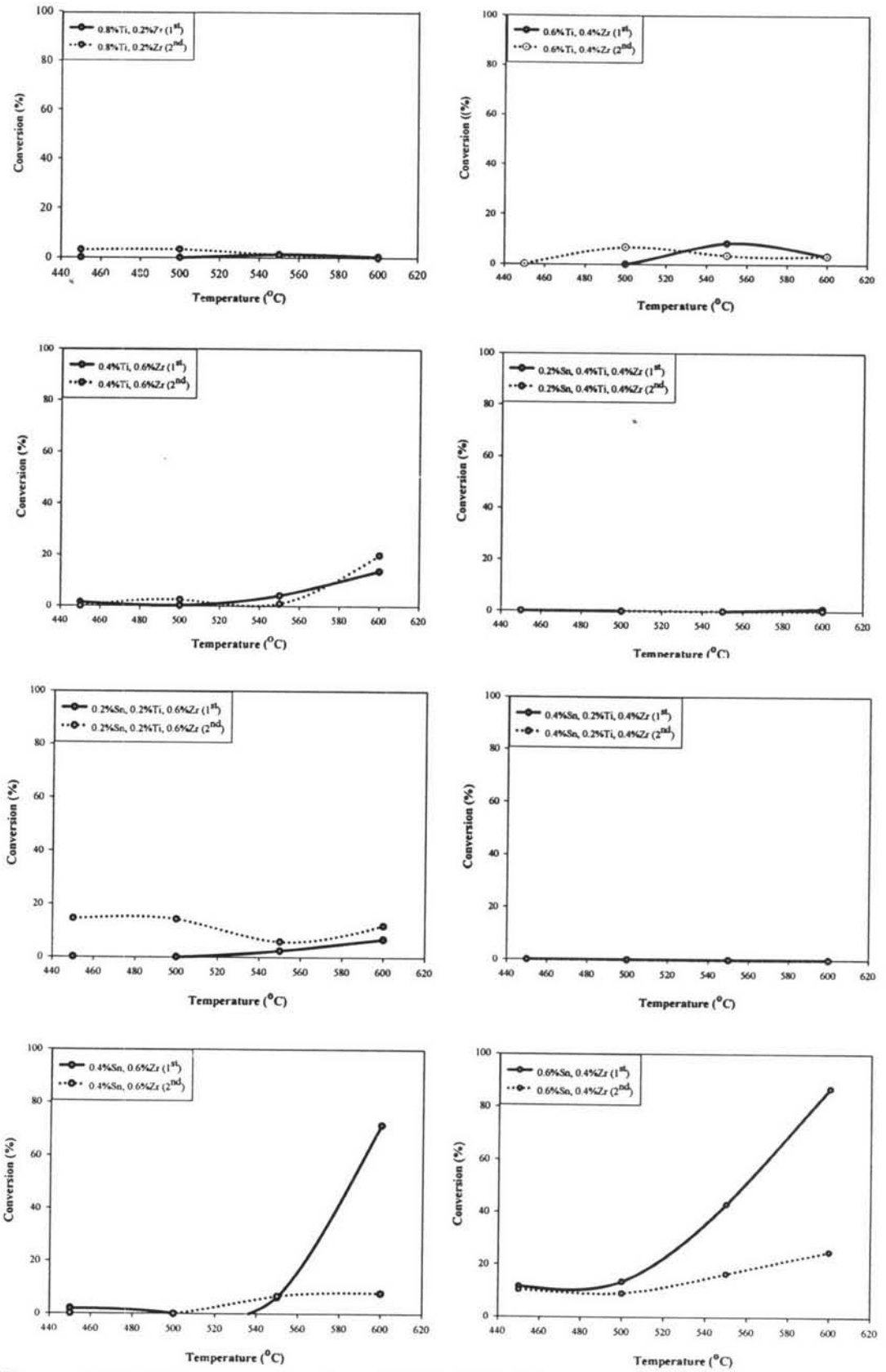

Figure 4.42 Methane conversion of C02, C03, C04, C09, C10, C14, C15, and C18 supported on γ-Al_2O_3 mixed with 5% ITQ-21.

From the previous results, it can be concluded that the addition of Sn could create the cluster of PdO, Originally exhibiting the high activity. However, it seems that tin also to larger PdO cluster at high reaction temperatures, resulting in the loss of activity for the second running cycle.

On the other hand, it seems that the addition of Ti did not promoted the occurrence of PdO film or clusters. So, the catalysts provide the low combustion activity for both first and second cycle.

4.3 Lead Characterizations

The catalysts were characterized using XRD and TPO techniques in order to investigate how the elements deposit on the surface, and explain the effects due to the loading of promoters and ITQ-21 on the combustion activity.

4.3.1 X-ray Diffraction (XRD)

The XRD patterns of the selected calcined catalysts at 500°C for 3 hours are illustrated in Figure 4.43. The XRD of Pd/γ-Al_2O_3 shows that the sample contains PdO with the characteristic peaks at 2θ = 34°and 41.95°. These PdO peaks are more intense and narrower than those of Pd/γ-Al_2O_3+ITQ-21, indicating that the PdO exists as a bigger and more crystalline species on the γ-Al_2O_3 support. The relative intensity of the PdO also decreased in the following order: Pd/γ-Al_2O_3, Pd/γ-Al_2O_3+ITQ-21, Pd/ITQ-21. Moreover, the pattern of ITQ-21 disappeared when loaded with Pd. This result suggests that the ITQ-21 structure would be destroyed by Pd. It was indicated that Pd would be present with Si, Al and Ge in the ITQ-21 as mixed oxides. When loading Pd onto the support mixture of γ-Al_2O_3 and ITQ-21, a small diffraction peak of PdO was observed as expected since a portion of the Pd was presented as mixed oxides with ITQ-21 while Pd supported on only γ-Al_2O_3 still appeared as PdO.

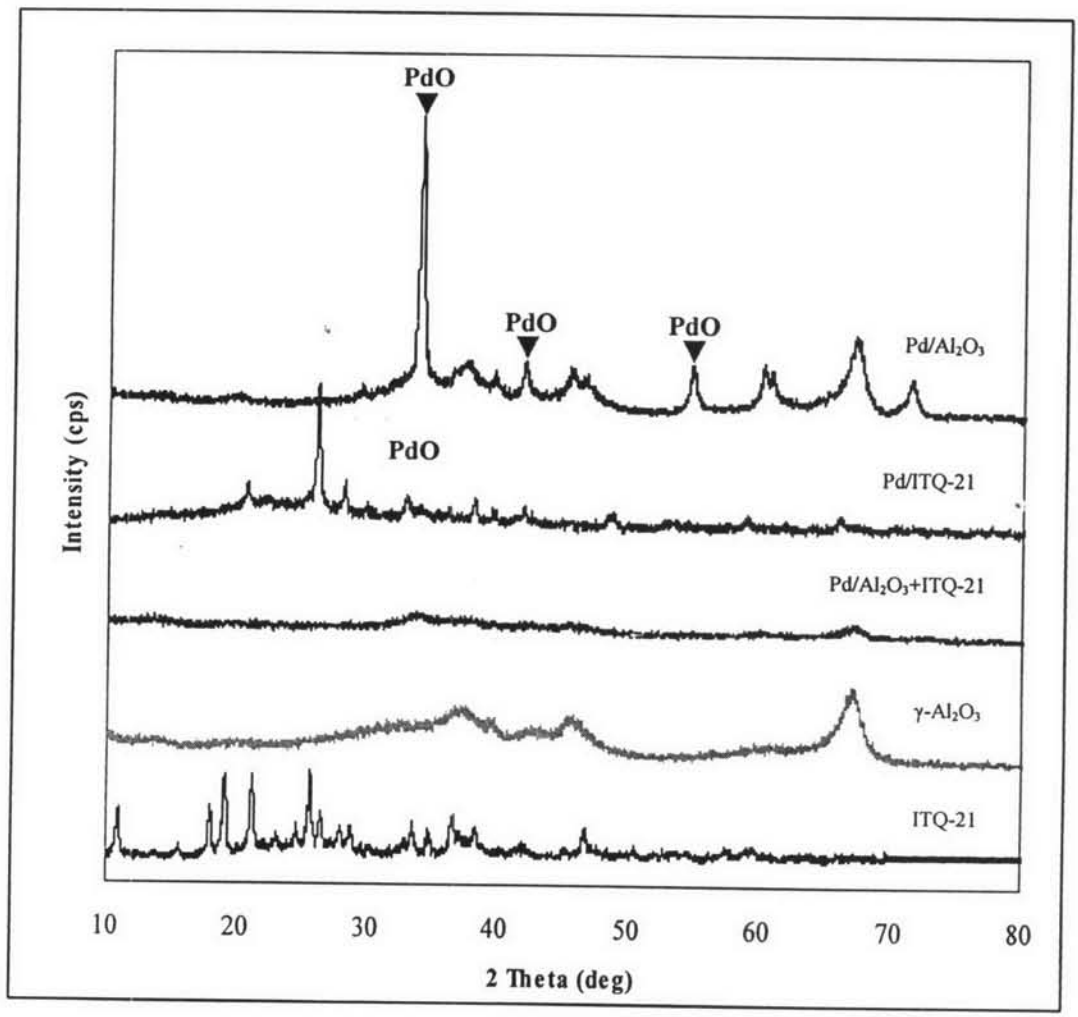

Figure 4.43 XRD patterns of fresh catalysts after calcination at 500°C for 3 hours.

4.3.2 Temperature Programmed Oxidation (TPO)

The purpose of the TPO experiments was to investigate the behavior of supported Pd catalysts under oxidative conditions. The results of the temperature-programmed oxidation are presented in Figure 4.44. TPO profile of Pd/γ-Al_2O_3 catalyst showed the desorption peaks representing oxygen release due to the decomposition of PdO into metallic Pd during the heating process. The onset temperature for these peaks was at 670°C, and it continued until 800°C as reported by Persson (2005). A small desorption peak was observed for the case of Pd supported on the mixture of γ-Al_2O_3 and ITQ-21, which is also in a good agreement with the XRD result. Because a portion of Pd formed as PdO while another formed mixed

oxide with ITQ-21, the oxygen quantity also decreased. The change on desorption temperature for Pd/γ-Al_2O_3+ITQ-21 from that of Pd/γ-Al_2O_3 suggests that the difference in Pd-O bond strengths occurs when changing the catalyst support, which would be due to the difference in PdO cluster sizes that have different metal-support interactions.

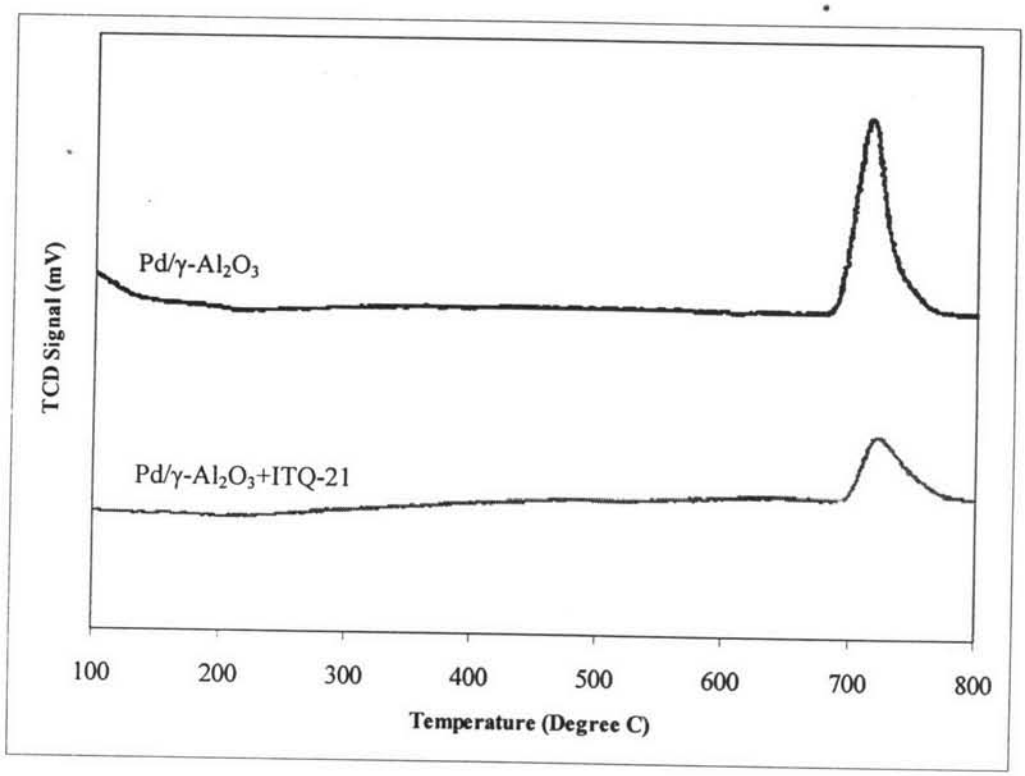

Figure 4.44 TPO profiles of fresh catalysts after calcination at 500°C for 3 hours.

4.3.3 Transmission Electron Microscope (TEM)

Figure 4.45 shows TEM images of the synthesis ITQ-21 zeolite, Pd/ITQ-21and Pd/Al_2O_3+ITQ-21. It was observed that the cubic shape of ITQ-21 has been destroyed to be needle-like mixed oxide after loading with Pd as depicted in Figure 4.45 (B). This result also substantiates the previous XRD result that indicates the change on the diffraction pattern after loading Pd onto ITQ-21.

For the case of Pd/Al_2O_3+ITQ-21, the TEM image (Figure 4.45 (C)) also agrees well with the proposed model that the mixed oxide should present with PdO on the Al_2O_3.

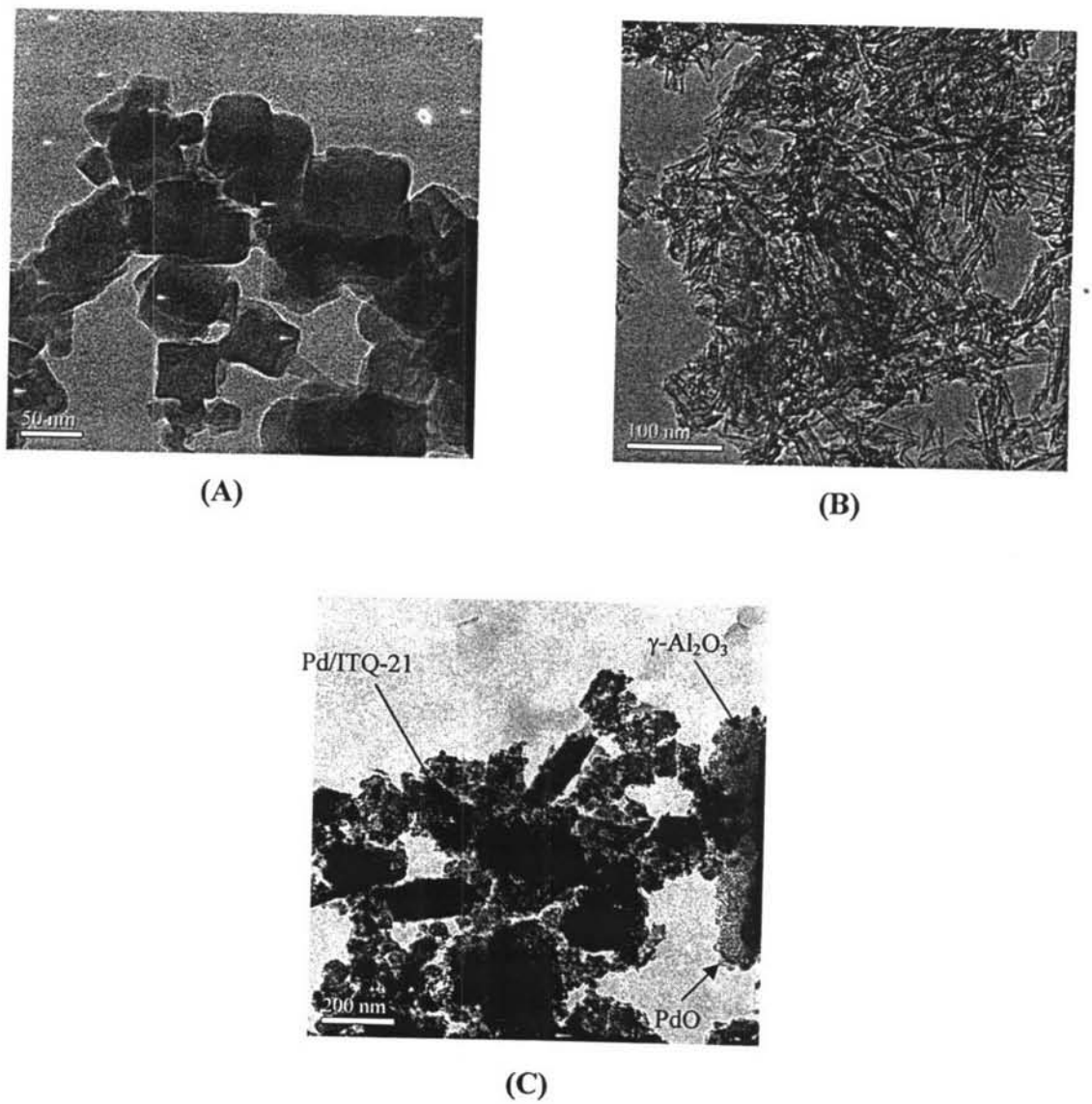

Figure 4.45 TEM images of (A) synthesized ITQ-21, (B) Pd/ITQ-21, and (C) Pd/γ-Al_2O_3+ITQ-21 after calcination at 500°C for 3 hours.